Recent results in spin physics.

R. Windmolders [a]

[a]Université de Mons-Hainaut,
B-7000 Mons, Belgium

E-mail:Roland.Windmolders@cern.ch

Recent results in polarized DIS are reviewed. Particular emphasis is placed on new measurements of transverse and longitudinal asymmetries, on the tests of the spin sum rules and on the analysis of the spin structure function g_1 in perturbative QCD at NLO.

1. INTRODUCTION

The aim of this introductory talk is to summarize the recent results in *polarized deep inelastic scattering.* After a brief reminder of experimental aspects specific to spin physics, we will review successively the new results on the transverse spin structure function g_2, the evaluation of the first moments Γ_1 for the proton and the neutron, the ongoing tests of the Gerasimov-Drell-Hearn sum rule, the fits of the Q^2 evolution of g_1 in perturbative QCD and the semi-inclusive asymmetries of charged hadrons. In general the data mentioned in this review have become public during the last year either in articles or in preprints. More recent (and therefore unpublished) data will be discussed in the spin session and summarized in the conclusions of this workshop.

2. GENERAL FEATURES OF POLARIZED DIS EXPERIMENTS

2.1. Spin asymmetries

In contrast with unpolarized experiments which measure cross sections, polarized DIS experiments measure spin asymmetries

$$A = \frac{\Delta\sigma}{2\overline{\sigma}} \qquad (1)$$

where $\Delta\sigma$ and $\overline{\sigma}$ are respectively the spin dependent and the spin averaged cross sections:

$$\Delta\sigma = \sigma^{\uparrow\downarrow} - \sigma^{\uparrow\uparrow},$$
$$\overline{\sigma} = (\sigma^{\uparrow\downarrow} + \sigma^{\uparrow\uparrow})/2$$

(the arrows correspond to the respective orientations of the beam and target particle spins).
The physics asymmetry A is equal to the measured one divided by the beam and target polarizations and by a factor f accounting for the fraction of polarizable nucleons in the target:

$$A = \frac{A_{meas}}{P_B P_T f} \qquad (2)$$

The uncertainties on the factors P_B, P_T and f are important sources of systematic error on the spin asymmetry A and on the spin structure functions.
The characteristics of recent (> 1990) spin experiments, including the average values of the beam and target polarizations and the corresponding errors, are listed in Table 1. Accuracies of 2 to 3 % are presently achieved for P_B and P_T.

In its most simplified form the dilution factor f is the ratio of the number of polarizable nucleons in the target by the total number of nucleons (e.g.$f = 3/17$ for $^{14}NH_3$). More accurately, the numbers of nucleons of various types must be weighted by the corresponding cross sections, e.g. in the case of a proton target

$$f = \frac{n_p \sigma^p_{tot}}{\sum_A n_A \sigma^A_{tot}} \qquad (3)$$

with the sum in the denominator running over all target nuclei.
A significant dependence of the dilution factor on the scaling variable x is generated by the variation of F_2^n/F_2^p vs. x as well as by the EMC effect

Table 1
Spin experiments 1990-99.

Exp.	Beam	Energy (GeV)	P_B	Target	P_T	Ref.
SMC	μ	100-190	$0.795 \pm 2.4\%$	C_4H_9OH (p) C_4D_9OD (d) NH_3 (p)	$0.86 \pm 3.2\%$ $0.51 \pm 2.0\%$ $0.89 \pm 2.7\%$	[1]
E142	e	19-23-26	$0.36 \pm 3.1\%$	^3He (n)	$\sim 0.33 \pm 7.0\%$	[2]
E143	e	10-16-29	$\sim 0.80 \pm 2.5\%$	$^{15}NH_3$(p) $^{15}ND_3$(d)	$\sim 0.70 \pm 2.5\%$ $\sim 0.25 \pm 4.0\%$	[3]
E154	e	48.3	$0.82 \pm 2.5\%$	^3He (n)	$\sim 0.38 \pm 5.0\%$	[4–6]
E155	e	48.3	$0.81 \pm 2.5\%$	$^{15}NH_3$ (p) ^6LiD (d)	$\sim 0.70 \pm 2.5\%$ $\sim 0.22 \pm 4.0\%$	[7–9]
HERMES	e	27	$0.40 - 0.65 \pm 3.0\%$	^3He (n) $\overline{H}$ (p)	$0.46 \pm 5.0\%$ $0.88 \pm 4.0\%$	[10–12]

modifying the cross section for nucleons bound in a nucleus.
In particular, the large radiative cross section at small x in nuclei sharply reduces the value of f for $x < 0.01$. In addition, a further decrease is produced by radiative corrections to the cross section on the polarized nucleon itself.
The measured asymmetry on a polarized proton target can be rewritten as

$$A_{meas} = P_B \cdot P_T \cdot f \frac{\Delta\sigma^p_{tot}}{\sigma^p_{tot}} = P_B \cdot P_T \cdot f \frac{\Delta\sigma^p_{tot}}{\sigma^p_{1\gamma}} \cdot \frac{\sigma^p_{1\gamma}}{\sigma^p_{tot}} \quad (4)$$

where $\sigma^p_{1\gamma}$ is the one-photon exchange cross section and σ^p_{tot} the total cross section including radiative effects. Due to radiative corrections, the spin dependent cross section $\Delta\sigma^p_{tot}$ slightly differs from $\Delta\sigma^p_{1\gamma}$ and the previous formula becomes

$$A_{meas} = \left(\frac{\Delta\sigma^p_{1\gamma}}{\sigma^p_{1\gamma}} + RC\right) P_B \cdot P_T \cdot f \cdot \left(\frac{\sigma^p_{1\gamma}}{\sigma^p_{tot}}\right) \quad (5)$$

showing that the "effective dilution factor" is

$$f' = f \cdot \frac{\sigma^p_{1\gamma}}{\sigma^p_{tot}}. \quad (6)$$

In the case of the SMC ammonia target, f' drops to about 0.05 at $x = 0.001$.
The effective dilution factor can however be significantly enhanced by restricting the sample to events where a hadron is detected in the final state [1]. In this case, the elastic tail does not contribute to the radiative corrections. The resulting increase of f' at low x largely compensates the reduction of the number of events in the data sample so that more accurate values of the asymmetry A are obtained. For the SMC kinematics, this condition was found to be true for $x < 0.02$. As an exemple, the x dependences of f' for inclusive and hadron tagged events in the SMC ammonia target are shown in Fig. 1. With hadron tagging, f' is of the order of 0.14 and approximatively constant at low x.

2.2. Virtual photon asymmetries and spin structure functions.

The spin asymmetry (1) is related to the virtual photon asymmetries A_1 and A_2 by the following relations which refer to configurations where the beam and target polarizations are parallel or perpendicular :

$$A_{\parallel} = \frac{d\sigma^{\uparrow\downarrow} - d\sigma^{\uparrow\uparrow}}{d\sigma^{\uparrow\downarrow} + d\sigma^{\uparrow\uparrow}} = D(A_1 + \eta A_2),$$

$$A_{\perp} = \frac{d\sigma^{\uparrow\rightarrow} - d\sigma^{\uparrow\leftarrow}}{d\sigma^{\uparrow\rightarrow} + d\sigma^{\uparrow\leftarrow}} = D\lambda(A_2 + \eta' A_1).$$

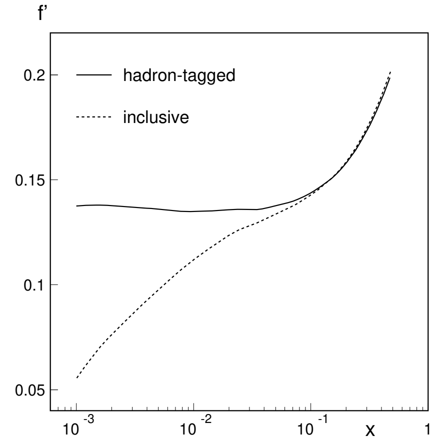

Figure 1. Effective dilution factor f' for hadron tagged and inclusive events from the SMC ammonia target.

The depolarization factor of the virtual photon

$$D = \frac{y(2-y)}{y^2 + 2(1-y)(1+R)} \tag{7}$$

depends on the ratio of the cross sections for longitudinally and transversely polarized photons $R = \sigma_L/\sigma_T$ while the other factors (λ, η, η') only depend on the event kinematics. The values of A_1 and A_2 are subject to the positivity conditions:

$$|A_1| < 1, \qquad |A_2| < \sqrt{R}.$$

The spin structure functions g_1 and g_2 are obtained from the virtual photon asymmetries A_1, A_2 and from the spin independent structure function F_1 :

$$\begin{aligned} A_1 \quad &= (g_1 - \gamma^2 g_2)/F_1, \\ A_2 \quad &= \gamma(g_1 + g_2)/F_1 \end{aligned}$$

with $\gamma^2 = 4M^2x^2/Q^2$.
When $A_\parallel$ and $A_\perp$ are both measured, as in the SLAC experiments, these relations fully determine g_1 and g_2. If only $A_\parallel$ is measured, g_1 can be obtained from the relation

$$g_1 = \frac{1}{1+\gamma^2}\left[\frac{A_\parallel}{D} + (\gamma - \eta)A_2\right]\frac{F_2}{2x(1+R)}. \tag{8}$$

In the kinematic range of the SMC experiment, the factors γ and η are both small, so that the contribution from the A_2 term can be safely neglected. At lower energies (as in the HERMES experiment), the previous formula is used with a parametrization of A_2.
The uncertainties on the factors P_B,P_T and f induce a normalisation error of about 4% on all values of A_1 and g_1. In addition,A_1 is affected by the uncertainty on $(1+R)$, which varies with the kinematic variables and becomes important in regions where R is poorly constrained. This uncertainty partially cancels out in g_1 but the spin structure function is further affected by the uncertainty on F_2 which is of the order of 4% (including a normalisation error of about 2%).

3. TRANSVERSE ASYMMETRIES

Exploratory measurements of A_2 have been performed by the SMC in 1994-1996 for the proton and deuteron targets. The transverse asymmetries were found to be much smaller than their positivity limit and compatible with zero within large errors [13,14]. A_2^n was first measured by E142 and also found compatible with zero [2].
The recent and more precise results from E143 [3] and E155 [7] show that A_2^p is positive and significantly different from zero in the range $0.2 < x < 0.7$ (Fig. 2):

$$\begin{aligned} \langle A_2 \rangle \quad &= 0.031 \pm 0.007 \quad (p), \\ \langle A_2 \rangle \quad &= 0.003 \pm 0.013 \quad (d), \\ \langle A_2 \rangle \quad &= -0.03 \pm 0.03 \quad (n). \end{aligned}$$

The structure function g_2 is of special interest because it provides a direct measurement of twist-3 contributions. It can indeed be decomposed as

$$g_2(x,Q^2) = g_2^{WW}(x,Q^2) + \overline{g}_2(x,Q^2) \tag{9}$$

where g_2^{WW} is the Wandzura-Wilczek term linear in g_1 and $\overline{g}_2$ an (almost) pure twist-3 contribution, except for a negligeable contribution originating from transverse parton polarization. The measured values of g_2 are in very good agreement with the Wandzura-Wilczek term (Fig. 3). As a consequence, the twist-3 matrix elements

$$d_n = 2\int_0^1 x^n \Big(\frac{n+1}{n}\Big)\overline{g}_2(x,Q^2)dx \tag{10}$$

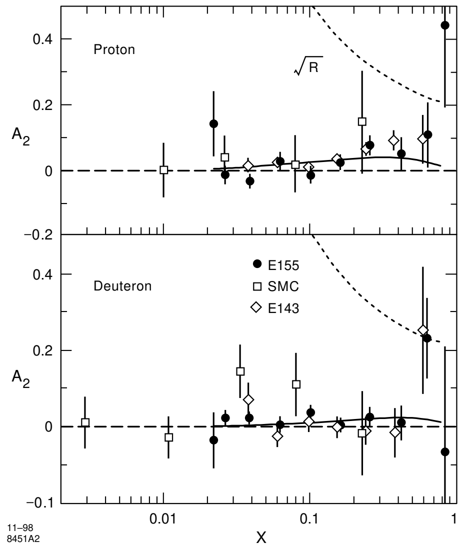

Figure 2. The asymmetries A_2 for proton and deuteron with their statistical errors [7]. The solid lines show the twist-2 contributions (corresponding to the WW term in g_2); the dashed lines show the positivity limits $\sqrt{R}$.

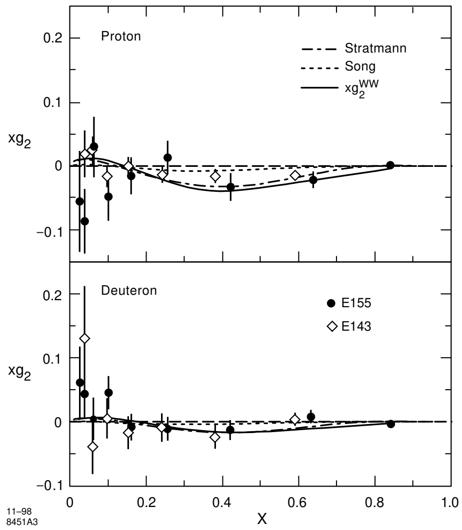

Figure 3. The structure function $xg_2(x)$ from the experiments E143 and E155 [7]. The errors are statistical. The full line shows the twist-2 contribution g_2^{WW}; the dashed and dash-dotted lines show model predictions from ref. [15] and [16].

derived from these data are consistent with zero. At $Q^2 = 5$ GeV^2, for the combined SLAC data their values are:

$$d_2^p = 0.007 \pm 0.004$$
$$d_2^n = 0.004 \pm 0.010.$$

The Burkhardt-Cottingham sum rule (BC):

$$\int_0^1 g_2(x)dx = 0 \tag{11}$$

is difficult to test on the existing data because the low x behaviour of g_2 is unknown. At $Q^2 = 5$ GeV^2 and for the range of the measurements ($0.02 < x < 0.8$), the combined SLAC data give values of -0.015 ± 0.026 and -0.010 ± 0.039 for the proton and the deuteron respectively, in agreement with the BC prediction.
The Efremov–Leader-Teryaev sum rule (ELT) predicts that the valence quark contribution to the second moment of $(g_1 + 2\ g_2)$ must be zero :

$$\int_0^1 x(g_1^V(x) + 2g_2^V(x))dx = 0. \tag{12}$$

Assuming I-spin symmetry for the sea, this prediction becomes

$$\int_0^1 x\Big[g_1 + 2g_2\Big]^{p-n} dx = 0 \tag{13}$$

and is easier to test than the BC prediction because it is less sensitive to the unmeasured contribution at low x. At the same Q^2 and for the same x range, the SLAC data give 0.003 ± 0.022, in good agreement with the ELT prediction. More accurate results on g_2 are expected in the near future from experiment E155X which is finishing its data taking at SLAC. These new data will constraint more precisely the values of the twist-3 matrix elements and may provide a discrimination between a large number of models which are presently all compatible with the data [7].

4. Γ_1 AND THE GDH SUM RULE

4.1. The first moment of g_1

The first moment of $g_1(x)$

$$\Gamma_1 = \int_0^1 g_1(x)dx \tag{14}$$

is by far the most intensively discussed topic in polarized DIS. The observation, made more than 10 years ago [17], that the value of Γ_1^p is significantly smaller than the one expected from the naive quark-parton model, assuming that the strange quarks do not contribute [18], has been at the origin of a new generation of experiments. The initial discovery has been confirmed by several new measurements, on the proton and on the neutron, and over a wide range of Q^2 (Fig. 4).

In the last years, special attention has been given

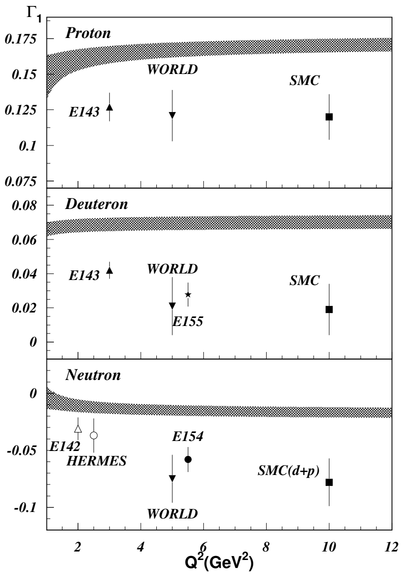

Figure 4. Values of the first moment Γ_1 of the spin structure function g_1 for the proton, deuteron and neutron. The shaded areas correspond to the naive expectations assuming no contribution from strange quarks.

to the low x extrapolation of the measured g_1 spectrum. At finite energy, Γ_1 is not a purely experimental quantity and must be split as

$$\Gamma_1 = \int_0^{x_d} g_1(x)dx + \int_{x_d}^{x_u} g_1(x)dx + \int_{x_u}^1 g_1(x)dx \tag{15}$$

where the second term covers the measured range of x. While the high x contribution is limited by the positivity condition $|A_1| < 1$ and by the small values of F_1, the contribution from the low x region is more difficult to evaluate and could, in principle, be large. In the past, it was estimated by a Regge extrapolation of g_1 at some low value of Q^2 (generally ~ 1 GeV^2). In recent analyses, this procedure is replaced by an extrapolation of the shape of g_1 fitted at next-to-leading order (NLO) in QCD, which will be discussed in a further section.

This new approach results in a significant shift of Γ_1 towards lower values (~ 0.015 for the proton). It also shifts to a lower value the singlet axial matrix element a_0 which is derived from Γ_1 under the assumption that the non-singlet part can be obtained from the $SU(3)$ coupling constants F and D as measured in hyperon β decay. For the proton and the deuteron, a_0 is related to Γ_1 by the formulas

$$\Gamma_1^p = \frac{1}{18}\, C_{NS}\,(3F + D) + \frac{1}{9}\, C_S\, a_0, \tag{16}$$

$$\frac{\Gamma_1^d}{1 - 1.5\omega_D} = \frac{1}{36}\, C_{NS}\,(3F - D) + \frac{1}{9}\, C_S\, a_0 \tag{17}$$

where C_S ans C_{NS} are the singlet and non-singlet QCD coefficient functions and ω_D is the probability for the deuteron to be in a D-state (~ 0.05). The change in Γ_1 due to the low x extrapolation reduces a_0 from the average value of 0.30 [3] to 0.18 ± 0.09 [9]. In the naive QPM approach shown by the shaded area in Fig.3, a_0 was expected to be identical to a_8 ($\simeq 0.58$).

4.2. The generalized GDH integral.

In general, spin structure functions depend on the variables ν and Q^2. The function $g_1(x)$ discussed so far is a scaling limit for large ν and Q^2:

$$M^2 \nu G_1(\nu, Q^2) \rightarrow g_1(x). \tag{18}$$

In order to study its behaviour at low Q^2 outside the scaling region, the first moment Γ_1 should therefore be rewritten as

$$\Gamma_1(Q^2) = Q^2 \int_{Q^2/2M}^{\infty} \frac{MG_1(\nu, Q^2)}{2} \frac{d\nu}{\nu}. \qquad (19)$$

The generalized Gerasimov-Drell-Hearn integral is defined by

$$I(Q^2) \simeq I_1(Q^2) = 16\pi^2\alpha \frac{\Gamma_1(Q^2)}{Q^2} \qquad (20)$$

and is of particular interest because its measured values (at finite Q^2) (Fig. 5) can be directly compared with the predictions of the GDH sum rule at $Q^2 = 0$:

$$I(0) = \int_{\nu_0}^{\infty} \Delta\sigma(\nu) \frac{d\nu}{\nu} = -\frac{2\pi^2\alpha}{M^2}\kappa^2 \qquad (21)$$

where κ is the anomalous magnetic moment of the nucleon. The predicted values are $-204\ \mu b$ for the proton and $-233\ \mu b$ for the neutron.

Although it was derived more than 30 years ago [19], the GDH sum rule has never been fully tested experimentally. A preliminary and partial result for the proton covering the range $0.2 < E_\gamma < 0.8$ GeV has been obtained last year ($-230 \pm 20\ \mu b$) [20]. Combined with model calculations for the missing contributions at low and high photon energy (-30 and $+25\ \mu b$ respectively), it yields a value in agreement with the sum rule. The experimental values of $I_1(Q^2)$ for the proton show a continuous increase with decreasing Q^2 down to $Q^2 = 0.5$ GeV^2. A rapid variation of the integral, including a change of sign, is thus required below this Q^2 if the data extrapolate smoothly to the sum rule prediction at $Q^2 = 0$. As shown in Fig. 5, the integral I_1 remains positive in the resonance region at the lowest value of Q^2 measured by E143. However, negative asymmetries are observed, as expected, in the Δ region [3] and a rapid change of the integral in the resonance region is predicted at lower Q^2 [21].

A similar behaviour is expected for the neutron. So far no measurements of the GDH sum rule have been made on a neutron target. The generalized GDH sum is being evaluated by experiment E94-010 at TJNAF using a polarized ^3He target [22]. The data presently collected cover the range $0.03 < Q^2 < 1.0$ GeV^2 and $0.7 < W < 2.4$ GeV.

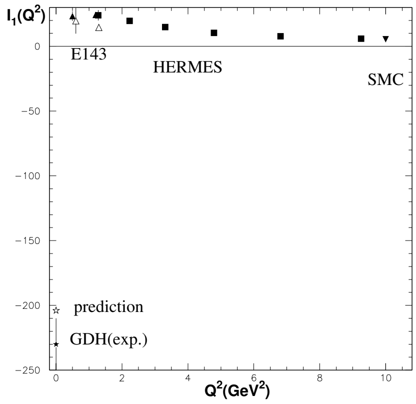

Figure 5. Values of the GDH integral $I_1(Q^2)$ (in μb) for the proton data from E143 [3], HERMES [12] and SMC [24] with the preliminary value measured at $Q^2 = 0$ [20] and the theoretical prediction. In the E143 data, the open triangles correspond to the resonance region, the full triangles to the DIS region.

5. NEW DATA ON A_1 AND g_1.

New data sets on the spin structure function g_1 have been published recently by Hermes [11], SMC [25] and E155 [9]. The deuteron data of E155 extend down to $x = 0.010$ and are in excellent agreement with previous data from E143 and SMC when evolved to a common Q^2. The Hermes data on hydrogen and the preliminary proton data from E155 also agree remarkably well with previous data sets (Fig. 6).

The new SMC data on proton (Fig. 7) and deuteron (Fig. 8) cover a limited range at low x and low Q^2 ($0.6 \cdot 10^{-4} < x < 0.8 \cdot 10^{-3}$, $0.02 < Q^2 < 0.2$ GeV^2) which has never been explored so far. The use of a calorimeter signal in the trigger and the requirement of a final state hadron in the analysis provide a clean sample of μN scat-

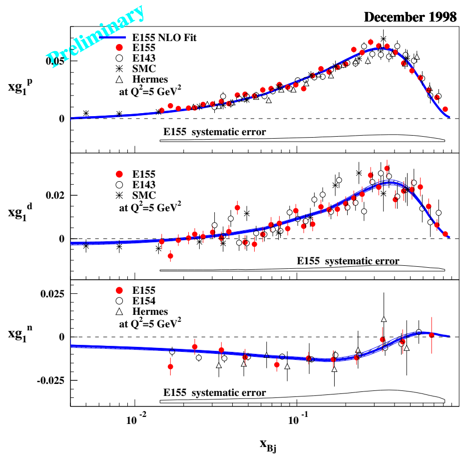

Figure 6. The structure functions $xg_1(x)$ at $Q^2 = 5\mathrm{GeV}^2$ for the proton, the deuteron and the neutron including preliminary results from E155 [9]. (The lowest SMC point for xg_1^p and xg_1^d is not shown). The continuous lines show the results of a QCD fit at NLO.

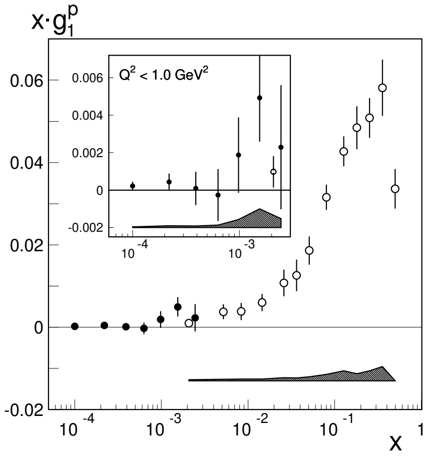

Figure 7. The values of xg_1 for the proton at the measured Q^2 obtained with the SMC low x trigger (filled circles) together with those from the SMC standard triggers (open circles) [25].

ters in a kinematic region where μ e scattering is the dominant process. No significant spin effects are observed in the newly accessed region. The values of g_1 shown in Figs.(7,8) have been calculated with F_2 values taken from the model of ref. [23]. The new data cover a very narrow range in W $(14 - 16$ GeV) and, for this reason, cannot be used to study the x dependence of g_1 at fixed Q^2 in a Regge-type fit.

6. QCD ANALYSIS OF SPIN STRUCTURE FUNCTIONS

6.1. Generalities

In QCD the quark-parton decomposition of the spin structure functions g_1

$$g_1^p(x) = \frac{1}{9}\Big[4\Delta u + \Delta d + \Delta s\Big],$$

$$g_1^n(x) = \frac{1}{9}\Big[\Delta u + 4\Delta d + \Delta s\Big].$$

is replaced by the general relation

$$g_1^{p(n)} = \frac{1}{9}\Big(C_{NS} \otimes \Big[\pm\, \Delta q_3 + \frac{1}{4}\Delta q_8\Big]$$

$$+ C_S \otimes \Delta\Sigma + 2N_f\ C_g \otimes \Delta g\Big), \qquad (22)$$

where C_{NS}, C_S, C_G are the non-singlet, singlet and gluon Wilson coefficients and the symbol $\otimes$ represents convolution with respect to x. In the case of 3 quark flavors discussed here, the non-singlet $(\Delta q_3, \Delta q_8)$ and singlet $(\Delta\Sigma)$ spin distributions are given in terms of quark spin distributions by

$$\Delta q_3 = \Delta u - \Delta d,$$
$$\Delta q_8 = \Delta u + \Delta d - 2\Delta s,$$
$$\Delta\Sigma = \Delta u + \Delta d + \Delta s.$$

The Q^2 evolution of the parton spin distributions is defined by the DGLAP equations

$$\frac{d}{dt}\Delta q_{NS} = \frac{\alpha_s(t)}{2\pi} P_{qq}^{NS} \otimes \Delta q_{NS}, \qquad (23)$$

$$\frac{d}{dt}\begin{pmatrix}\Delta\Sigma \\ \Delta g\end{pmatrix} = \frac{\alpha_s(t)}{2\pi}\begin{pmatrix}P_{qq}^S & P_{qg}^S \\ P_{gq}^S & P_{gg}^S\end{pmatrix} \otimes \begin{pmatrix}\Delta\Sigma \\ \Delta g\end{pmatrix},$$

where $t = \log Q^2/\Lambda^2$ and P_{ij}^S are the polarized splitting functions. In this section, we will discuss fits of the Q^2 evolution at next-to-leading order and review the results obtained in four different

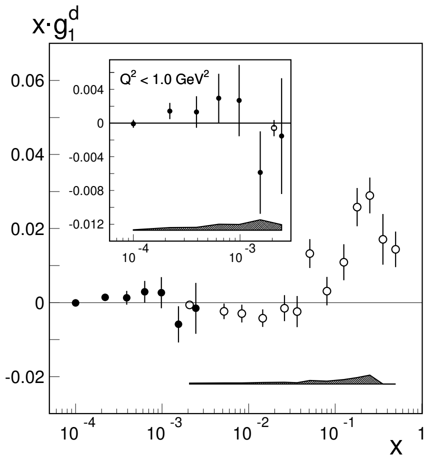

Figure 8. The values of xg_1 for the deuteron at the measured Q^2 obtained with the SMC low x trigger (filled circles) together with those from the SMC standard triggers (open circles) [25].

analyses performed by Altarelli, Ball, Forte and Ridolfi ("ABFR",[26]), Leader, Sidorov and Stamenov ("LSS",[27]), the E154 collaboration [6] and the SMC [24].
In all cases the procedure starts with simple parametrizations of the polarized pdf's at some initial arbitrarely choosen Q_i^2. The pdf's are then evolved using the DGLAP equations (23) to the Q^2 of every data point and the resulting g_1 recalculated. The obtained values are compared to the measured ones and the parameters in the initial pdf's are adjusted in order to minimize the resulting χ^2.
The results of the fit are used for several purposes. First of all, they provide a way to evolve the measured values of g_1 to a common Q^2 for the full range of the measurements. In the past, results were evolved to a common Q^2 under the assumption that the ratio g_1/F_1 is independent of Q^2, a hypothesis which has no theoretical support but is still compatible with the data for $Q^2 > 1$ GeV^2.
The fitted shape of g_1 at fixed Q^2 is also used to extrapolate into the regions out of the range of the experiments. At low x, the resulting shape is quite different from the one obtained with a Regge type extrapolation and leads to different estimates of Γ_1.
Fits of g_1 are one of the few sources of information about polarized parton distributions. They are thus extremely useful to test or improve the existing parametrizations.
The four QCD analyses discussed here are based on similar (although not identical) data sets and differ mainly by different choices concerning the form of initial parametrizations, the definition of parameters and the initial Q_i^2. The fitting procedure and the handling of systematic errors are also quite different.
In the ABFR and SMC fits, the polarized pdf's are introduced explicitely, in the form

$$\Delta q(x, Q_i^2) = \eta N(\alpha, \beta, a) x^\alpha (1-x)^\beta (1+ax) \quad (24)$$

where η, α, β and a are free parameters (some of them may be fixed in some cases). In the LSS and E154 fits, the polarized pdf's are defined in relation with the unpolarized ones

$$\Delta q(x, Q_i^2) = \eta N(\alpha, \beta) x^\alpha (1-x)^\beta q(x, Q_i^2) \quad (25)$$

which are taken from the MRST parametrization for LSS [28] or from the GRV parametrization for E154 [29] of the valence and sea quark distributions. In this approach, a further assumption has to be made, since inclusive spin asymmetries are not sensitive to valence and sea quarks.
$\Delta\overline{s}$ can be obtained, at least in principle, from the difference

$$\Delta\overline{s} = (1/6)(\Delta\Sigma - \Delta q_8). \quad (26)$$

Assuming flavor symmetry breaking of the sea in the form $\Delta\overline{u} = \Delta\overline{d} = \lambda\Delta\overline{s}$, one may then derive the valence quark spin distributions conditionnally on λ :

$$\begin{aligned} \Delta u_v(\lambda) &= \Delta u_v(\lambda = 1) - 2(\lambda - 1)\Delta\overline{s}, \\ \Delta d_v(\lambda) &= \Delta d_v(\lambda = 1) - 2(\lambda - 1)\Delta\overline{s}. \end{aligned} \quad (27)$$

The consistency of the results for different choices of λ with the above equations has been tested by LSS [27]. It is worth mentionning that the introduction of unpolarized pdf's (as in eqn.(25)) provides a satisfactory description of the data with

a smaller number of free parameters.
Fits in the four analyses have been performed in moment space. The SMC analysis has used the same fitting algorithm as the ABFR analysis but the results have been cross-checked with an independent program where the fit is done in $(x-Q^2)$ space.

6.2. Factorization scheme

At next-to-leading order, the splitting functions, the coefficient functions and, in general, the parton distributions depend on the renormalization and factorization schemes, while physical observables remain scheme independent. In the $\overline{MS}$ scheme, the gluon density does not contribute to the first moment Γ_1 because the first moment of the gluon coefficient function is zero. In this scheme, the singlet axial matrix element a_0 (Eqs. (16-17)) is identical to the first moment of the singlet distribution $\Delta\Sigma$ and depends on Q^2.
The Adler-Bardeen scheme (AB) is a modified $\overline{MS}$ scheme where $\Delta\Sigma$ is changed by terms proportionnal to $\alpha_s(Q^2)\Delta g(x,Q^2)$. These corrections may be large even at high Q^2 because $\int_0^1 \Delta g(x,Q^2)dx \simeq \left[\alpha_s(Q^2)\right]^{-1}$. The singlet distributions in the AB and $\overline{MS}$ schemes are related by

$$\Delta\Sigma(x,Q^2)_{AB} = \Delta\Sigma(x,Q^2)_{\overline{MS}} + N_f\frac{\alpha_s(Q^2)}{2\pi}\int_x^1 \frac{dy}{y}\Delta g(y,Q^2) \tag{28}$$

while the gluon and non-singlet distributions remain unchanged. Consequently, the first moment of the singlet distribution $\Delta\Sigma_{AB}$ differs from a_0:

$$a_0(Q^2) = \Delta\Sigma(1)_{AB} - N_f\frac{\alpha_s(Q^2)}{2\pi}\Delta g(1,Q^2) \tag{29}$$

and is independent of Q^2.
It has been pointed out [27] that the AB scheme is a particular case of a family of schemes differing by higher moments $\Delta\Sigma(n)$, $(n \geq 2)$.
Fits in different schemes are expected to give consistent results, i.e. the different fitted singlet distributions should be in agreement with eqn.(28).

6.3. Positivity conditions

The condition that the difference of cross sections for total spin 1/2 and total spin 3/2 has to be smaller than the sum

$$|\sigma_{1/2} - \sigma_{3/2}| \leq \sigma_{1/2} + \sigma_{3/2} \tag{30}$$

leads to the well known limits $|A_1| \leq 1$ or $|g_1(x,Q^2)| \leq F_1(x,Q^2)$. At leading order, these conditions imply that

$$|\Delta q_i(x,Q^2)| \leq q_i(x,Q^2) \tag{31}$$

for all quark flavors. The same relation can be established for the gluon by considering Higgs production by the process $g + g \rightarrow H$. At next-to-leading order, these relations, which correspond to the probabilistic interpretation of polarized pdf's, are no longer valid. Their generalisation has been studied in ref.[26] and leads to correlated boundary conditions on the moments $(\Delta\Sigma(N), \Delta g(N))$. These conditions could be used as additionnal constraints in the determination of polarized pdf's.

6.4. Results on moments

The results on the moments of the pdf's obtained in the four different analyses are summarized in Fig. 9.
The first one, Δq_3, is often fixed in the fits at the nominal value of (F+D) in order to satisfy the Bjorken sum rule [30]. When it is left as a free parameter, the fitted value provides a test of this sum rule. The results shown in the plot (part (a)) indicate that the data confirm the Bjorken sum rule within an accuracy of about 10%. The second result quoted for the SMC analysis corresponds to a partial fit of the non-singlet part $g_1^p - g_1^n$. Such a fit has the adventage that it requires only few parameters and is independent of the gluon. The result is consistent with the global fit but slightly less accurate, due to the limited amount of data presently usable in this non-singlet fit.
The values of the singlet axial matrix element a_0 (part (b) of the plot) are consistent in the four analyses. They are also consistent for fits done in the $\overline{MS}$ and AB schemes, as expected for a scheme independent quantity. The errors are significantly larger for the derivations in the AB scheme, due to the additionnal systematic error related to the gluon. It can also be seen that systematic errors have been treated differently in the four analyses. The effect of changes in the

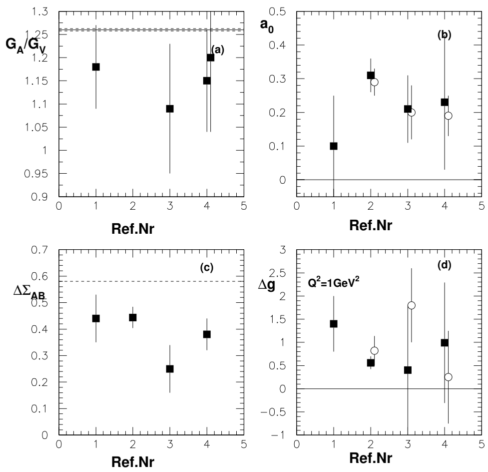

Figure 9. (a) Values of G_A/G_V; (b) values of the singlet axial matrix element a_0; (c) values of the singlet first moment in the AB scheme $\Delta\Sigma_{AB}$; (d) values of $\Delta g(Q^2 = 1\ \mathrm{GeV}^2)$ in the four analyses (1=ABFR, 2=LSS, 3=E154, 4=SMC). Results obtained in the $\overline{MS}$ scheme are shown as open circles, results obtained in the AB scheme as full squares. The quoted errors are the statistical and systematic errors combined in quadrature, however the theoretical uncertainty is not included in the LSS errors. See text for the duplicated SMC point in part (a).

factorization and renormalization scales by factors varying between 0.5 and 2.0 are included in the error quoted by the SMC analysis, as well as the effect of changes in the form of the input parametrizations (24). By comparison, the errors quoted by the LSS analysis appear largely underestimated.

The first moment of the spin singlet in the AB scheme (part (c) of the plot) averages around 0.40. The comparison with the values of a_0 shows the increase due to the gluon contribution to the nucleon spin. It is however clear that the value of $\Delta\Sigma_{AB}$ remains significantly below the quark-parton model expectation of 0.58. In other words, the present data suggest that the gluon accounts for about half of the difference between the measured values of Γ_1 and their QPM expectations (Fig. 4) leaving room for other effects, such as orbital momentum.

The first moment of the gluon spin distribution evaluated at $Q^2 = 1\ \mathrm{GeV}^2$ (part (d) of the plot) is of the order of 1. The same remarks as above apply for the errors. It is also observed that the evaluations made in the 2 factorization schemes differ by about one standard deviation but that the sign of these differences is not the same in all analyses. This clearly shows the limit of attempts to determine the gluon contribution from inclusive measurements where the role of the gluon is restricted to the Q^2 evolution.

6.5. Results on parton spin distributions.

Contrary to $\Delta q_3(x)$ which is unambiguously defined by the difference $g_1^p(x) - g_1^n(x)$, the contribution to g_1 from $\Delta q_8(x)$, $\Delta\Sigma(x)$ and $\Delta g(x)$ can only be disentangled by their different Q^2 evolution. The range in Q^2 is presently defined by the SLAC experiments ($E = 20$ GeV) and the SMC experiment ($E = 190$ GeV) and corresponds to a factor of about 6 at fixed x. It is thus expected that only the largest contribution to g_1 will be reasonnably well constrained by the data.

Fig. 10 shows the fitted $g_1^d(x)$ at the Q^2 of the SMC data together with its non-singlet and singlet components. It can be seen that the singlet term $x\Delta\Sigma$ (evaluated in the $\overline{MS}$ scheme) closely follows the variation of xg_1^d, from negative values at small x to a maximum around $x = 0.25$.

The singlet distribution appears thus to be strongly constrained by the measured values of g_1^d and will be well determined by the fit. Results from different fits [24,27] show indeed remarkable agreement.

The previous figure also suggest that the determination of the small $\Delta q_8(x)$ contribution will be much more difficult. In general, the first moment of Δq_8 is fixed to the value obtained from hyperon β decay (= 3F - D). In addition, its shape is often assumed to be the same as $\Delta q_3(x)$. The latter assumption has no theoretical justification and is motivated only by the lack of constraint in the

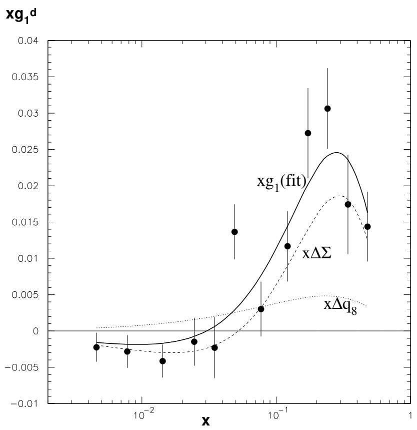

Figure 10. The fitted $g_1^d(x)$ with the SMC data at their measured Q^2; also shown are the contributions from the singlet term (in the $\overline{MS}$ scheme) and from the non-singlet term Δq_8.

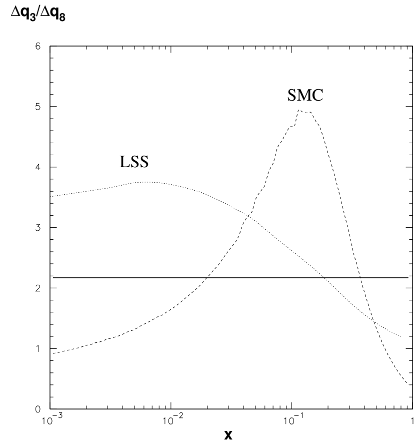

Figure 11. The fitted ratio $\Delta q_3(x)/\Delta q_8(x)$ at $Q^2 = 1\text{GeV}^2$ as obtained in the LSS and SMC fits where the shape of $\Delta q_8(x)$ is left free. The horizontal line shows the ratio of the 2 moments.

fit. As an illustration, we show in Fig. 11 the ratio $\Delta q_3/\Delta q_8$ obtained in the LSS and in the SMC fits where the shape of $\Delta q_8(x)$ was left free. The deviations with respect to the ratio of moments (shown by the horizontal line) are completely different in the 2 fits and result mainly from the constraints imposed by the analytical form of the input distributions. In conclusion, no significant information on Δq_8 can be derived from the inclusive data with their present precision.
The same could be said about the shape of the gluon distribution which is affected by very large statistical and systematic errors. Fig. 12 shows the fitted pdf's in the AB scheme as obtained in the SMC analysis [24]. The statistical error is much larger for the gluon than for the other distributions because the gluon only contributes to g_1 through the Q^2 evolution. For the same reason, the gluon is strongly affected by the "theoretical" error originating from the variation in renormalization and factorization scales.

As mentionned before, the fitted shape of $g_1(x)$ is extrapolated down to $x = 0$ in order to evaluate the moments Γ_1. Fig. 13 shows the extrapolation of g_1^p at $Q^2 = 1\text{GeV}^2$. The spin structure function becomes negative below $x = 0.001$ (i.e. slightly below the lowest data point). The drop towards large negative values when x tends to zero is driven by the singlet term (also shown in the figure). It should be noticed that the polarized pdf's at x below the range of the data do not influence the fit results (as shown in eqn.(22), the value of g_1 at a given x only depends on the pdf's at *higher* x). The validity of the extrapolation to $x = 0$ therefore rests on the assumption that the shape of polarized pdf's which was found to describe the data remains valid at lower x. Future measurements of g_1^p below $x = 0.001$, for instance from the polarized HERA collider [31], would be needed to confirm the change of sign suggested by the extrapolation.

7. HADRON ASYMMETRIES

Measurements of semi-inclusive asymmetries for positively and negatively charged hadrons, when combined with the inclusive asymmetries and analyzed in the framework of the quark-parton model, provide the spin distributions of

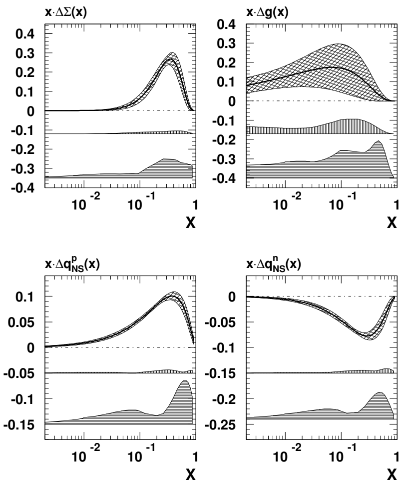

Figure 12. Polarized parton distributions at $Q^2 = 1\text{GeV}^2$ from the SMC fit in the AB scheme (singlet, gluon, non-singlet for the proton and for the neutron) [24]. The bands with crossed hatch show the statistical uncertainty as obtained in the fit while the vertically and horizontally hatched bands correspond to the experimental and theoretical uncertainties respectively.

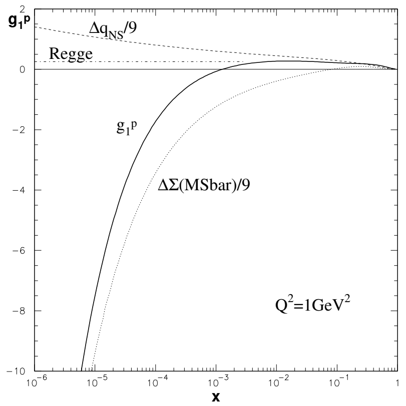

Figure 13. The extrapolated $g_1^p(x)$ at $Q^2 = 1$ GeV^2 from the SMC QCD fit at NLO compared to a Regge type extrapolation. Also shown are the extrapolated singlet (in $\overline{MS}$ scheme) and non-singlet terms.

valence and sea quarks. The SMC analysis [32] has shown that the u valence quarks are polarized positively ($\Delta u_v = 0.77 \pm 0.13$) and that their polarization increases with x while the d valence quarks are polarized negatively ($\Delta d_v = -0.52 \pm 0.17$). No significant polarization was found for sea quarks ($\Delta\overline{q} = 0.01 \pm 0.05$).

The semi-inclusive asymmetries collected by HERMES on the proton target are in good agreement with those from SMC and improve considerably the statistical precision (Fig. 14). Combined with the less precise asymmetries on the ^3He target, these new data lead to the valence and sea quark spin distributions shown in Fig. 15. The SMC results are confirmed with statistical errors reduced by half for the u valence quark and the sea quarks. A comparable improvement is expected for the d valence quark when the data presently collected on a deuterium target will become available.

In general, the analysis of semi-inclusive spin asymmetries has been limited to the framework of the quark-parton model. A QCD analysis at next-to-leading order based on inclusive and semi-inclusive data has been attempted in ref. [34]. The emergence of more precise semi-inclusive data, possibly also for identified particles, will make this approach more relevant in the future and may help answer some of the pending questions in the QCD analysis of g_1.

The difficulty to determine the gluon spin distribution from the Q^2 evolution of g_1 has lead to an increased interest for reactions dominated by photon-gluon fusion, a process which gives access to Δg with a large analysis power. The COMPASS experiment, planned to start at CERN in the year 2000, intends to determine Δg from open charm production [35] using the full virtual photon flux down to $Q^2 = 0$ and also from events where a pair of high p_t hadrons is produced.

The SLAC experiment E155 has studied the

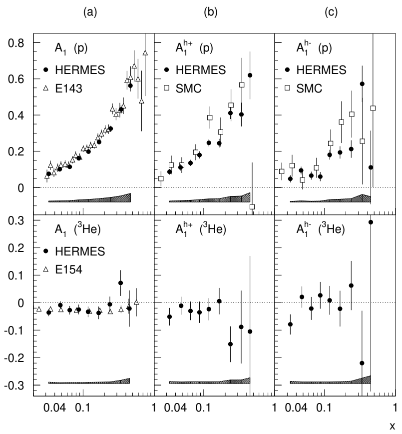

Figure 14. Inclusive asymmetries (left side), semi-inclusive asymmetries for positive hadrons (center) and for negative hadrons (right side) measured by HERMES. The upper and lower plots are for the hydrogen and ^3He target respectively. Data from previous experiments are shown for comparison.

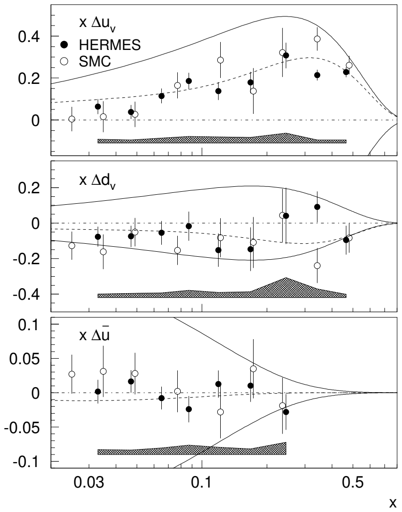

Figure 15. Distribution of the valence and sea quark spin distributions derived from the inclusive and semi-inclusive asymmetries measured by HERMES. The values obtained previously by SMC in the same x range are shown for comparison. The full lines show the limits defined by spin independent quark distribution; the dashed lines are the prediction of the G-S parametrization [33].

reactions

$$\gamma p \longrightarrow (\text{hadron})^{\pm}\ X,$$
$$\gamma d \longrightarrow (\text{hadron})^{\pm}\ X$$

with circularly polarized photons [8]. In these reactions, the sensitivity to the gluon spin distribution could also be enhanced due to the photon-gluon process. Small asymmetries significantly different from zero have been observed for positive and negative hadrons produced on the proton target while the asymmetries on the deuteron target are consistent with zero. The interpretation of these results remains difficult because the event kinematics is unknown and many different processes may contribute.

8. CONCLUSIONS

The field of spin physics has been characterized in 1998/99 by a rather limited amount of new data but very extensive work to finalize the analysis of previous experiments. Besides the ongoing analyses of spin structure functions in perturbative QCD, there has been a diversification of interest towards the non-perturbative low Q^2 region and photoproduction, including the long awaited test of the Gerasimov-Drell-Hearn sum rule.

Hadron asymmetries have become a major subject of interest due to the precise data obtained by HERMES.

The transverse asymmetry A_2 is now well measured and found to be different from zero for the proton. Its compatibility with the twist-2 contribution will be further investigated with the most recent SLAC data.

It is a pleasure to thank my colleagues and friends from the SMC for many fruitful discussions over many years. I also like to thank colleagues from other collaborations who have kindly provided information about their experiment during the preparation of this talk, in particular A. Brüll (HERMES), E. Hughes (E155), Z.-E. Meziani (E94-010), S. Rock (E155) and A. Thomas (GDH).

REFERENCES

1. SMC, B. Adeva et al., Phys. Rev. **D58** (1998) 112001.
2. E142, P.L. Anthony et al., Phys. Rev. **D54** (1996) 6620.
3. E143, K. Abe et al., Phys. Rev. **D58** (1998) 112003.
4. E154, K. Abe et al., Phys. Rev. Lett. **79** (1997) 26.
5. E154, K. Abe et al., Phys. Lett. **B404** (1997) 377.
6. E154, K. Abe et al., Phys. Lett. **B405** (1997) 180.
7. E155, P.L. Anthony et al., hep-ex/9901006.
8. E155, P.L. Anthony et al., hep-ph/9902412.
9. E155, P.L. Anthony et al., SLAC-PUB-8041 (March 1999).
10. HERMES, K. Ackerstaff et al., Phys. Lett. **B404** (1997) 383.
11. HERMES, A. Airapetian et al., Phys. Lett. **B442** (1998) 484.
12. HERMES, K. Ackerstaff et al., Phys. Lett. **B444** (1998) 531.
13. SMC, D. Adams et al., Phys. Lett. **B336** (1994) 125.
14. SMC, D. Adams et al., Phys. Lett. **B396** (1997) 338.
15. X. Song, Phys. Rev. **D54** (1996) 1955.
16. M. Stratmann, Z. Phys. **C60** (1993) 763.
17. EMC, J. Ashman et al., Phys. Lett. **B206** (1998) 364.
18. J. Ellis and R.L. Jaffe, Phys. Rev. **D9** (1974) 1444; *ibid* **D10** (1974) 1669.
19. S.B. Gerasimov, Sov. J. Nucl. Phys. **2** (1966) 430; S.B. Drell, A.C. Hearn, Phys. Rev. Lett. **16** (1966) 908.
20. H. Dutz, Proc. 13th Int. Symp. on High Energy Spin Physics, Protvino (Sept. 1998).
21. D. Drechsel et al., hep-ph/9810480-v2 (26 Jan 1999).
22. Z.E. Meziani, Proc. of this workshop.
23. B.Badelek and J. Kwiecinski, Phys. Lett. **B295** (1992) 263.
24. SMC, B. Adeva et al., Phys. Rev. **D58** (1998) 112002.
25. SMC, B. Adeva et al., CERN-EP/99-61 (April 1999).
26. G.Altarelli et al., Acta Phys. Pol. **B29** (1998) 1145, hep-ph/9803237;
    S.Forte et al., hep-ph/9808462;
    G.Altarelli et al., Nucl. Phys. **B534** (1998) 277.
27. E.Leader et al., Phys. Rev. **D58** (1998) 114028; E. Leader et al., Phys. Lett. **B445** (1998) 232.
28. A.D. Martin et al., hep-ph/9803445.
29. M. Gluck et al., Z. Phys. **C67** (1995) 433.
30. J.D. Bjorken, Phys. Rev. **148** (1966) 1467; *ibid.* **D1** (1970) 1376.
31. "Physics with polarized protons at HERA", DESY-proceeding-1998-01, (February 1998).
32. SMC, B. Adeva et al., Phys. Lett. **B420** (1998) 180.
33. T. Gehrmann and W. J. Stirling, Phys. Rev. **D53** (1996) 6100.
34. D. de Florian et al., Phys. Rev. **D57** (1998) 5803.
35. COMPASS proposal, CERN/SPSLC 96-14, SPSC/P297; CERN/SPSLC 96-30 (May 1996).